BULLETIN OF THE POLISH ACADEMY OF SCIENCES
TECHNICAL SCIENCES, Vol. 70(5), 2022, Article number: e143104
DOI: 10.24425/bpasts.2022.143104

Effect of optical illumination and magnetic field on the electroconductive and polarization properties of clathrate GaSe<$CS(NH_2)_2$<$C_{14}H_{10}$>>, synthesized under lighting

Fedir IVASHCHYSHYN[1,2*], Vitalii MAKSYMYCH[2], Dariusz CALUS[1], Dariya MATULKA[2], Piotr CHABECKI[1], and Andrii KUNYNETS[2]

[1] Czestochowa University of Technology, Al. Armii Krajowej 17, 42-200 Częstochowa, Poland
[2] Lviv Polytechnic National University, Bandera Str. 12, Lviv, 79013, Ukraine

Abstract. GaSe⟨$CS(NH_2)_2$⟨$C_{14}H_{10}$⟩⟩ clathrate with a hierarchical subhost⟨host⟨guest⟩⟩ type architecture was formed under illumination and its electrically conductive properties were studied. The method of impedance spectroscopy studied the frequency behavior of real and imaginary parts of complex total impedance in the range of 10^{-3}–10^6 Hz. Measurements were performed under normal conditions, in a permanent magnetic field (220 kA/m), or under light illumination (for a standard solar spectrum of AM 1.5 G total available power is 982 W/m^2). Structure of the impurity energy spectrum at the Fermi level was investigated by the method of thermostimulated discharge in the temperature range from 240 to 340 K. Using Jebol-Pollack theoretical approaches based on impedance spectra, parameters of the impurity energy spectrum were calculated, such as the density of states at the Fermi level, the jump radius, the scatter of trap levels near the Fermi level and the real density of deep traps. As evidenced by studies, illumination during clathrate synthesis forms an internal electret polarization, which leads to abnormal behavior of the photoresistive effect and to the appearance of the memristive effect. The imposition of a permanent magnetic field during measurement of complex resistance leads to the appearance of quantum capacitance.

Key words: GaSe; thiourea; anthracene; clathrate; impedance spectroscopy; quantum capacitance; memristive effect.

1. INTRODUCTION

The intensive development of electronics has prompted the search for new functionally hybrid inorganic/organic materials designed at the level of nanoscale objects. Organic molecules are increasingly often acting as such materials because, unlike inorganic compounds, they have a wide range of extraordinary properties. Supramolecular complexes constructed by means of weak interactions most often represent self-assembled systems and complexes based on the lock-key principle [1–3]. Exactly for this reason, due to the weak interaction (ionic-dipolar interactions, Van der Waals interactions, π-interactions, hydrogen bonding, hydrophobic effects) between the host and guest materials, it is possible to maintain the identity of both components. Ensuring the nanosize of structural elements opens up completely new properties and approaches to studying the materials. Significant changes in the parameters of phase transitions for nanostructured materials [4–6], quantum enhancement of sensory sensitivity to external physical fields [7–9] or a giant increase of dielectric constant [10, 11] are all examples of such effects. At the same time, the magnitude and nature of these changes depend both on the type of matrix and guest content and on the method of their synthesis, for example, exposure to illumination.

It is possible to form more complicated clathrate complexes of the subhost⟨host⟨guest⟩⟩ type by using intercalation technologies. This approach opens up brand new possibilities for the design of nanostructured inorganic/organic materials. Using inorganic matrices not only makes it possible to structure supramolecular complexes, but also provides reliable anticoagulant matrix isolation of nanosystems and stabilization of their properties [12, 13]. This technology also allows for application of physical fields to achieve a certain ordering of organic molecules, modifying their properties in the process of clathrate formation. For example, in [14], illumination during clathrate formation forms a photoelectric polarization of the guest component, which consequently leads to the appearance of a huge photo-dielectric effect, i.e. a combination of high dielectric permittivity values with $\mathrm{tg}\delta > 1$ at low frequencies, thus demonstrating the possibility of creating a quantum accumulator – the appearance of the electromotive force when a constant magnetic field is applied, whose value at room temperatures reaches 2 V. Quantum mechanisms will make it possible to accumulate electrical energy of a much higher density. Authors of [15, 16] predict that this will give impulse to significant development of renewable energy systems. Such extraordinary properties of

*e-mail: fedirivashchyshyn@gmail.com

Manuscript 2022-06-17, revised 2022-08-04, initially accepted for publication 2022-08-26, published in October 2022.

hierarchical clathrates undoubtedly actualize the further development of research. First of all, thus entails studying the dependence of physical processes on the type of matrix of the host and supramolecular complex of the host-guest type, as well as elucidation of the influence on their properties of technological conditions of synthesis with the application of external physical fields. Therefore, the aim of this work is to continue the study of the effect of light on the photoelectric properties of the clathrates obtained.

2. BASIC CONCEPT AND METHOD OF EXPERIMENT

Semiconductor single crystal GaSe was used as the subhost matrix. Grown by means of the Bridgman–Stockbarger method, the single crystal has a pronounced layered structure and p-type conductivity (Fig. 1). The anisotropy of its properties allows researchers to look for unique (2D) electronic properties such as large electron mobility, quantum Hall effect, anomalous optical response, or induced states of zero resistance [17, 18]. Due to the peculiarities of the structure, the layered crystal of group A_3B_6 is a promising thermoelectric material with a high value of potential field [19]. It can be used in various fields of electronics [20, 21] and it can also work as a matrix of 2D guest positions, the latter being particularly important in our case.

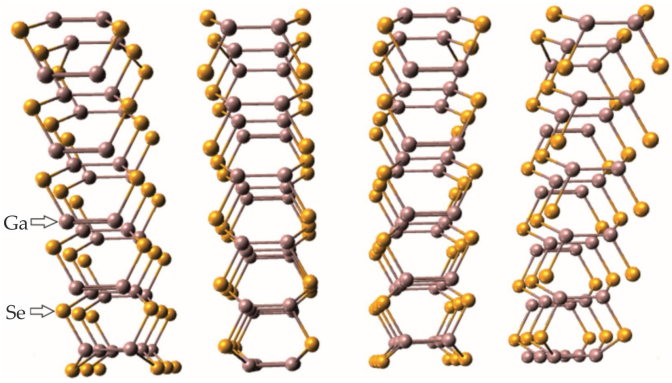

Fig. 1. Spatial representation of GaSe structure

Thiourea ($CS(NH_2)_2$) was the supramolecular cavitand (Fig. 2). Thiourea is also called thiocarbamide, 2-thiourea or isothiourea [22]. The C=S bond distance is 1.71 Å, the C–N distances average stands at 1.33 Å [23]. The thiourea host is formed by hydrogen bonding and it can include a variety of guest molecules of appropriate size and shape [24]. It can act as an intermediate host due to strong intermolecular hydrogen bonds between the acidic protons of the NH_2 groups and oxygen or sulfur atoms of neighboring molecules. As a result, a chiral spiral hollow tube is formed from urea molecules with a minimum Van der Waals diameter of 5.5÷5.8 Å. The dipole moment of thiourea is $18.86 \cdot 10^{-30}$ C · m and relative permittivity of thiourea is 2.224 [25]. Due to its nonlinear optical properties, thiourea is now widely used in the electronics industry, for example, in polarizing filters, electronic optical shutters and electronic modulators, and also as a component in electro-optical and electro-acoustic devices. In addition, thiourea is widely used in various electrochemical processes [26]. Guests with a small cross-section can enter this tube [27, 28].

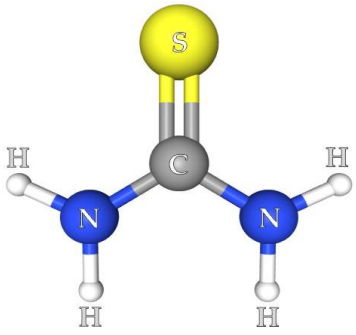

Fig. 2. Molecular structure of thiourea

Anthracene ($C_{14}H_{10}$) was chosen as a guest (Fig. 3) [28, 29]. It is a well-known organic photoelectret, and its properties in the macrostructured state are well studied. In contrast, changes in the mechanisms of photoelectret polarization during transition to a nanostructured state, as well as changes of the guest content in clathrates, are practically not studied today.

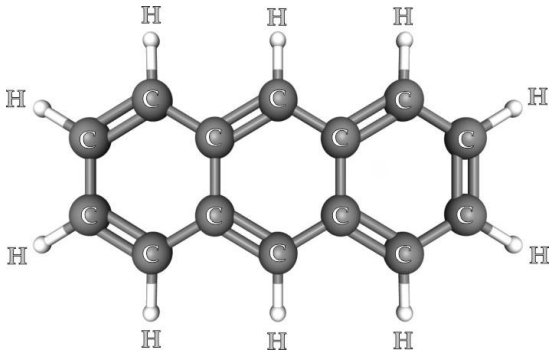

Fig. 3. Molecular structure of anthracene

The supramolecular compound $CS(NH_2)_2\langle C_{14}H_{10}\rangle$ was formed by mixing saturated solutions of the respective components in the molar ratio of 1:1. The solvent was ethanol 96%.

The GaSe crystal matrix adaptation to the incorporation between the layers of the supramolecular complex $CS(NH_2)_2\langle C_{14}H_{10}\rangle$ was realized by applying the intercalation-deintercalation three-stage technology of crystal engineering described in sufficient detail in our previous work [30]. The extension of the crystal matrix of GaSe monocrystal after the second stage was 4-fold. During the third technological stage, the supramolecular complex was introduced by dipping the 4-fold expanded GaSe single crystal into the formed solution of thiourea and anthracene for 24 h in order to ensure the intercalation process. The sample was then removed from the solution and allowed to dry at room temperature to remove the solvent. At this stage, to ensure photoelectricity of the supramolecular component, the sample was illuminated by an AM 1.5 G standard solar spectrum simulator lamp with a total available power of 982 W/m^2. The evaporation process with simultaneous illumination proceeded for 6 hours. The sample was illuminated in the direction normal to the plane monocrystal layers of the GaSe.

In order to study the mechanisms of current passage and their changes during the introduction of the supramolecular complex $CS(NH_2)_2\langle C_{14}H_{10}\rangle$ in the GaSe semiconductor matrix, the impedance spectra were measured using the measuring complex "AUTOLAB" of ECO CHEMIE (Netherlands) in the C direction of the monocrystalline. For this, indium contacts were deposited upon both facets (perpendicular to the crystallographic axis C). The amplitude of the measuring signal was 5 mV and frequency range was $10^{-3} \div 10^{6}$ Hz. Taking into account that conductivity along the layers is much higher than conductivity across the layers, we will assume that the current will flow through the crystal in the direction of the C axis. Impedance spectrum measurements were performed under normal conditions, in the permanent magnetic field (220 kA/m), or under light illumination (for a standard solar spectrum AM 1.5 G total available power is 982 W/m^2). A permanent magnet was chosen as the source of the permanent magnetic field so it did not affect the measuring complex and did not introduce additional variable signals during measurement. The action of the reciprocal physical fields was oriented in the direction of transmission of the measuring signal (in the direction of the C axis). This measurement geometry was chosen for the purpose of the collinear action of the permanent magnetic field and the current of the measurement signal.

Thermally stimulated discharge spectra were measured in a short-circuit mode under linear heating at a rate of 5°C/min in order to establish the structure of the electronic energy topology of impurity levels. The contacts applied to the crystal were connected to an ammeter with large input resistance. During the heating process, the corresponding current was fixed and the values were recorded with some time interval. Due to the linearity of heating, the relaxation processes are investigated as a function of temperature, but not time. This is an advantage because the nature of various relaxation processes in this method is revealed rather quickly.

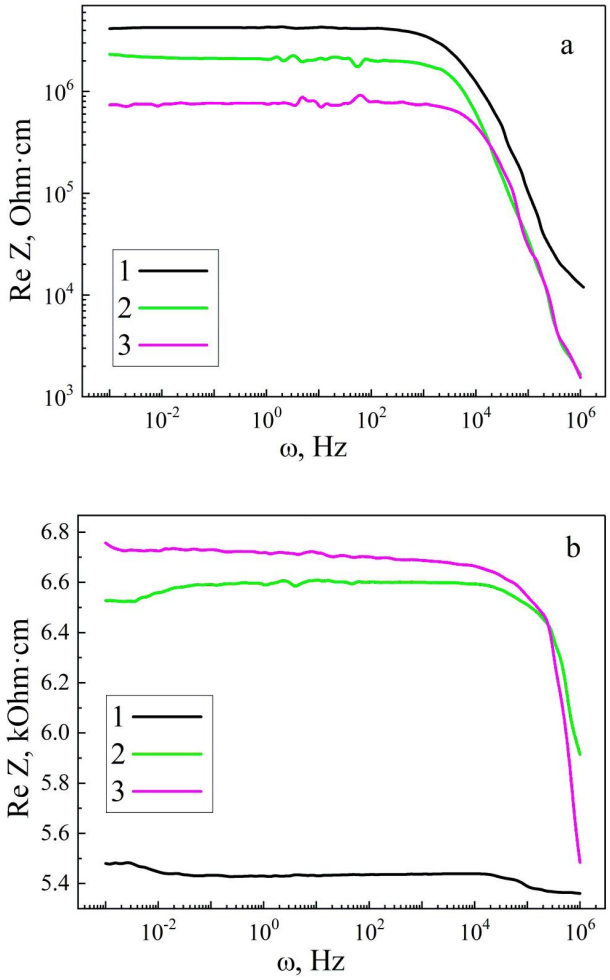

Fig. 4. Frequency dependences of the real component of the specific complex impedance of a 4-fold expanded matrix GaSe (a) and clathrate $GaSe\langle CS(NH_2)_2\langle C_{14}H_{10}\rangle\rangle$ (b). Measurements were performed under normal conditions (1), in applied permanent magnetic field (2) and under light illumination (3)

3. RESULTS AND DISCUSSION

Let us then begin the analysis of the conductivity properties of the initial 4-fold expanded matrix GaSe and the clathrate $GaSe\langle CS(NH_2)_2\langle C_{14}H_{10}\rangle\rangle$ formed on its basis. For this purpose, the frequency dependences of the real part of the complex resistance $\mathrm{Re}Z(\omega)$, measured for the original and intercalated matrices, are presented in Fig. 4.

Thus, the initial 4-fold expanded matrix of GaSe under normal measurement conditions is characterized by the charge transfer stage resistance behavior typical of this type of objects. $\mathrm{Re}Z(\omega)$ takes on a frequency-independent behavior over a wide frequency range, which indicates the main contribution to the conductivity of thermally excited carriers (Fig. 4a, curve 1). Beginning from the frequency of 10^3 Hz, $\mathrm{Re}Z(\omega)$ passes to frequency-dependent behavior, which indicates the inclusion of carrier hopping conduction with energies close to the Fermi level E_F. Frequency-dependent conductivity can be written as follows:

$$\sigma(\omega) \equiv \mathrm{Re}\widehat{\sigma}(\omega) \sim \omega^n, \qquad (1)$$

where index n can take values within $0.64 \leq n \leq 1.0$. In this case, starting from the frequency of 10^3 Hz, the conductivity is subject to functional dependence $\sigma(\omega) \sim \omega^{0.8}$. The applied permanent magnetic field leads to a 2-fold decrease in the real part of complex resistance $\mathrm{Re}Z$ (Fig. 4a, curve 2) as a result of the Zeeman delocalization of carriers. The appearance of medium-frequency oscillations, which appear due to the activation of small traps capable of holding current carriers for a time comparable with the half-period of the measuring signal, is different from the initial behavior of $\mathrm{Re}Z(\omega)$ in this case. Illumination leads to a more than 5-fold decrease in $\mathrm{Re}Z$ (Fig. 4a curve 3) because the single crystal of GaSe is photosensitive. Similarly to the case of the permanent magnetic field, a medium-frequency oscillatory behavior of $\mathrm{Re}Z(\omega)$ is visualized, caused by photoactivation of the traps capable of holding current carriers for a time comparable to the half-period of the measuring signal.

The insertion of the supramolecular complex $CS(NH_2)_2\langle C_{14}H_{10}\rangle$ between the layers of a 4-fold expanded matrix of GaSe leads to a 1000-fold decrease in $\mathrm{Re}Z$ caused by an in-

crease in the concentration of free charge carriers due to the guest subsystem (Fig. 4b, curve 1). We can assume that under the conditions of the formed clathrate $GaSe\langle CS(NH_2)_2\ \langle C_{14}H_{10}\rangle\rangle$ under the action of light illumination, photoelectric states were formed, which are appropriately placed in the band gap [31]. In general, this causes an increase in the Fermi level [32], and hence an increase in conductivity of the material. In this case, the dependence of $\mathrm{Re}Z(\omega)$ loses frequency independence in the low-frequency range ($10^{-3} \div 10^{-2}$ Hz), taking on a monotonically decreasing character. It should also be noted that the high-frequency boundary frequency of change of the conduction mechanism has been shifted by over an order of magnitude, to the high-frequency region. In contrast to the initial 4-fold expanded matrix of GaSe, the permanent magnetic field leads to a 20% increase in $\mathrm{Re}Z(\omega)$ due to the Zeeman localization of carriers. At the same time, and more interestingly, it changes the frequency genesis at the low-frequency region $\mathrm{Re}Z(\omega)$ to the opposite – monotonically increasing. This low-frequency behavior of $\mathrm{Re}Z(\omega)$ may be related to the quantum capacitance (C_q) caused by the discretization of the energy spectrum and the finite tunneling times [33].

As we know, in the general case, capacitance C is defined as

$$C = \frac{\mathrm{d}Q}{\mathrm{d}V}. \tag{2}$$

For low-dimensional structures, a change of the charge Q caused by the applied electrostatic field V is

$$Q = e\sum_n f(E_n), \tag{3}$$

where e is the magnitude of the electronic charge, and

$$f(E_n) = \frac{1}{\exp\left(\dfrac{E_n - \mu + eV}{kBT}\right) + 1} \tag{4}$$

is the Fermi–Dirac distribution, μ is a chemical potential or Fermi level, k_B is Boltzmann's constant and T is temperature, while V is the local electrostatic potential and E_n is the quantum state of the system.

Equation (2) can also be represented as:

$$C = \frac{\mathrm{d}Q}{\mathrm{d}V} \;\Rightarrow\; -e\frac{\mathrm{d}Q}{\mathrm{d}\mu}. \tag{5}$$

Thus, V and μ up to a factor identically determine the capacitance. The effect of its change can be realized by the potential shift, since the increase in V shifts the zone upwards and thus lifts E_F.

The dispersion law of the current carriers in semiconductors near the bottom of the conduction band or near the top of the valence band is well described by parabolic dependence in the case of some crystals of orthogonal symmetry. We have considered a plate of thickness l cut out along the OZ axe of the crystal.

The permanent magnetic field applied to the plate ensures an addition to the dimensional quantization discreteness of states:

$$E_{\nu,n} = \hbar\omega_B(\nu + 1/2) + \frac{\hbar^2\pi^2}{2m_l^* l^2}n^2, \qquad \nu = 0,1,2,\ldots, \quad n = 1,2,3,\ldots. \tag{6}$$

where ω_B is the cyclotron frequency; m_l^* is the effective mass along the OZ axe of the crystal; $\hbar$ is Planck's constant/2π while ν and n are quantum numbers.

The Fermi level E_F is localized in the middle of the band gap E_g of the semiconductor nanoplate with symmetric conduction and valence bands. We choose its position as a datum point. Charge caused by the field applied was determined by the following formula [34]:

$$Q = e\sum_{n=1}^{\infty}\left\{f\left(E_n + \frac{E_g}{2} + eV\right) - f\left(E_n + \frac{E_g}{2} - eV\right)\right\} \tag{7}$$

and quantum capacitance was determined by means of:

$$C_q = -\frac{e^2}{4k_BT}\sum_{n=1}^{\infty}\left\{\cosh^{-2}\left(\frac{E_n + E_g/2 + eV}{2k_BT}\right) + \cosh^{-2}\left(\frac{E_n + E_g/2 - eV}{2k_BT}\right)\right\}. \tag{8}$$

As stated above, here summation is over all quantum states of the semiconductor nanoplate. The Fermi level is fixed in the middle of the band gap and the filling of states in both zones is due to the "tails" of the Fermi–Dirac distribution.

On the basis of the theoretical formulas obtained, appropriate calculations were carried out using the Maple applied mathematical package. We established the qualitative dependence of quantum capacity of such a nanoobject on the position of the Fermi level and the magnitude of the magnetic field.

The magnetic field which is normally applied to the plate leads to additional quantization of band states and of its plane [33]. It is interesting to note an important practical aspect of quantum capacitance (C_q) generation by the permanent magnetic field. An anomalous photoresistive behavior of the $GaSe\langle CS(NH_2)_2\langle C_{14}H_{10}\rangle\rangle$ clathrate is obtained under illumination, and $\mathrm{Re}Z$ increases by 24%. The mechanism of this phenomenon is most likely to be associated with photoinduced adhesion centers on inorganic/organic hetero-boundaries.

Using the theory of jump conduction proposed by M. Pollak and T.H. Geballe [35], which takes into account the jumping of charge carriers between states localized in space due to their interaction with phonons, we obtained the following expression for the real part of conductivity:

$$\sigma(\omega) = \frac{\pi}{96}e^2k_BT\alpha^{(-5)}N_F^2\omega\left[\ln\left(\frac{\nu_\Phi}{\omega}\right)\right]^4, \tag{9}$$

where e – electron charge; N_F – density of states at Fermi level; α – constant of decrease of the wave function of the localized carrier and ν_Φ – phonon frequency. Using the formula and having experimentally measured values of $\sigma(\omega)$, we determined the density of states at Fermi level N_F.

According to the theory of hopping conductivity in alternating current, the average carrier hopping time τ with absorption or emission of a phonon is determined by the expression below:

$$\tau^{-1} = \nu_\Phi \exp(-2\alpha R), \tag{10}$$

where R – hopping distance. Experimentally τ^{-1} is the average frequency at which the law is executed with $\omega^{0.8}$. The value τ^{-1} can be defining experimentally and then the average distance of jump R can be calculated from the last formula.

Knowing the magnitude of N_F and R from the ratio:

$$\frac{4}{3}\pi R^3 N_F \frac{1}{2} J = 1, \tag{11}$$

the scatter of trap levels J near the Fermi level can be estimated. This in turn enables the following formula:

$$N_t = N_F J, \tag{12}$$

estimating the real density of deep traps N_t. The obtained values of the corresponding values, according to the presented calculations, are shown in Table 1. Abbreviations N_C, M_F and L stand for normal conditions, constant magnetic field and illumination, respectively.

Table 1

Band spectrum parameters before and after insertion of $\langle CS(NH_2)_2\langle C_{14}H_{10}\rangle\rangle$ into GaSe

Structure		$N_F \cdot 10^{44}$, $J^{-1}m^{-1}$	$R \cdot 10^{-8}$, m	$J \cdot 10^{-22}$, J	$N_t \cdot 10^{22}$, m^{-3}
4-fold expanded GaSe matrix	NC	1.13	3.00	1.58	1.78
	MF	1.35	2.77	1.67	2.25
	L	1.63	2.58	1.71	2.78
GaSe$\langle CS(NH_2)_2\langle C_{14}H_{10}\rangle\rangle$ clathrate	NC	8.26	2.55	3.50	2.89
	MF	8.13	2.58	3.42	2.78
	L	9.52	2.64	2.72	2.59

As we can see from the table presented, the insertion of the guest component leads to an almost 8-fold increase in the density of states at the Fermi level, a decrease in the average jump distance, more than a 2-fold increase in the spread of trap levels near the Fermi level and more than a 1.5-fold increase in deep trap center density. In general, we obtain a sufficiently good correlation of the above mechanisms of the current passage with theoretically calculated results.

For experimental confirmation of the results obtained, the thermally stimulated discharge currents were measured for the initial 4-fold expanded GaSe matrix and the $\langle CS(NH_2)_2\langle C_{14}H_{10}\rangle\rangle$ clathrate formed on its basis (Fig. 5). The main difference between the spectra is that, for the initial 4-fold expanded GaSe matrix, hetero-charge relaxation is observed, in contrast to the $\langle CS(NH_2)_2\langle C_{14}H_{10}\rangle\rangle$ clathrate, which is characterized by only homo-charge relaxation. The next difference, of no less importance, is the transformation of the narrow-band nature of the spectrum at temperatures from 270 K to 300 K into a quasi-continuous spectrum. The obtained results of measurements of thermally stimulated discharge currents confirm the previously obtained results and their interpretation.

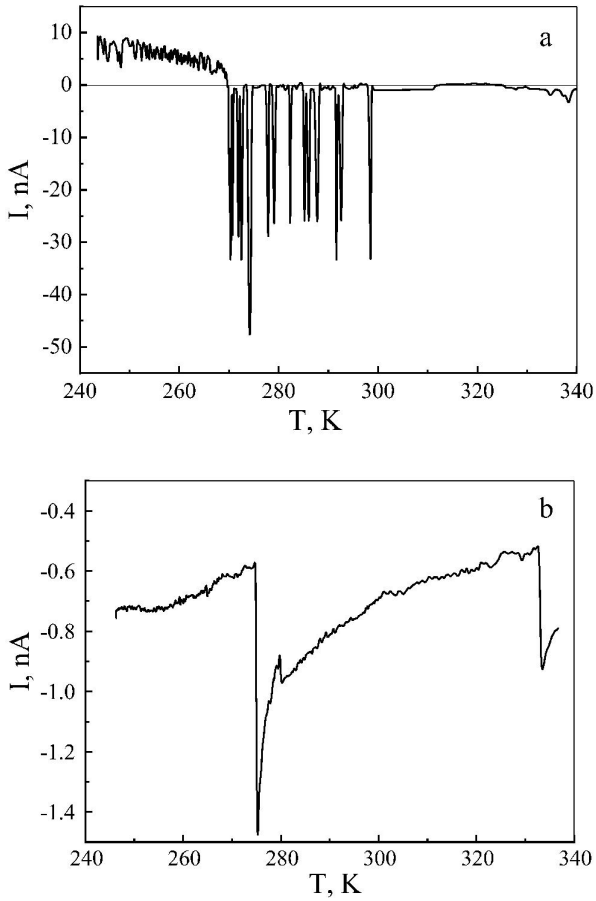

Fig. 5. Thermally stimulated discharge current spectra measured for 4-fold expanded matrix of GaSe (a) and clathrate GaSe$\langle CS(NH_2)_2\langle C_{14}H_{10}\rangle\rangle$ (b)

Corresponding changes in the energy structure of the GaSe$\langle CS(NH_2)_2\langle C_{14}H_{10}\rangle\rangle$ clathrate will lead to significant changes in its polarization properties. The analysis of the image component of the complex impedance $-\mathrm{Im}Z$ with frequency was performed (Fig. 6) for this purpose.

For the initial 4-fold expanded GaSe matrix (curve 1 in Fig. 6a), a characteristic pronounced main relaxation maximum is observed in the vicinity of the frequency of $4{\cdot}10^3$ Hz, which corresponds to the mobility of charge carriers at a given temperature. The permanent magnetic field leads to a significant decrease in the height of the main relaxation maximum (curve 2 in Fig. 6a) and to its shift to higher frequencies. This indicates a small increase in the mobility of current carriers in this case, due to the effect of the magnetic field on the spin subsystem. Under the influence of illumination there is a significantly greater decrease in the intensity of the main relaxation maximum (curve 3 in Fig. 6a) and its shift toward higher frequencies can be observed. This result is caused by the influence of the photoelectric effect and an increase in the mobility of carriers.

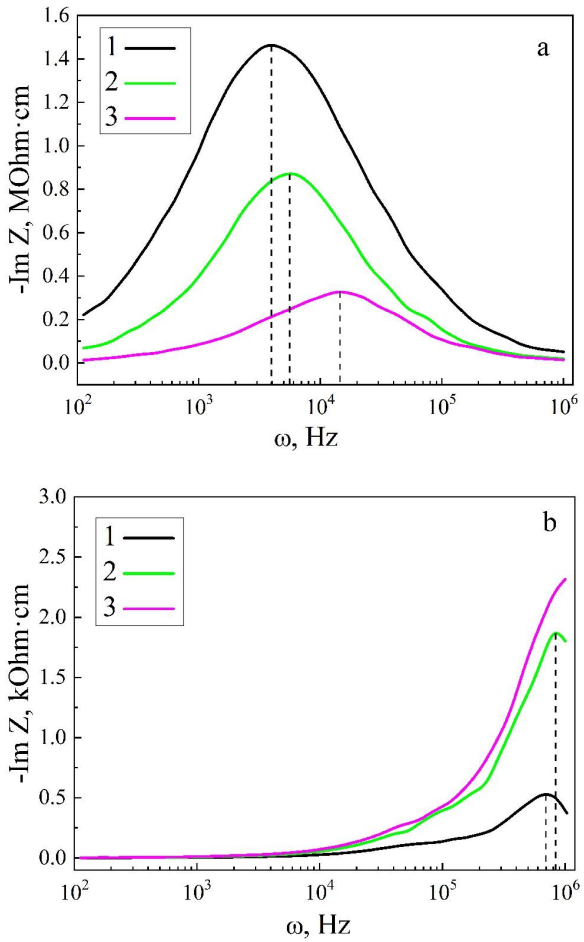

Fig. 6. Frequency dependences of the image component of the specific complex impedance of 4-fold expanded matrix GaSe (a) and clathrate $\langle CS(NH_2)_2\langle C_{14}H_{10}\rangle\rangle$ (b). Measurements were performed under normal conditions (1), in applied permanent magnetic field (2) and under light illumination (3)

The insertion of the guest component and the formation of clathrate $\langle CS(NH_2)_2\langle C_{14}H_{10}\rangle\rangle$ leads to more than 1000-fold reduction of $-\mathrm{Im}Z(\omega)$ (Fig. 6b). In this case, the main relaxation maximum shifts toward much higher frequencies in the vicinity of $6.5{\cdot}10^5$ Hz. This indicates the dominant contribution of carriers of the guest component with higher mobility. The imposition of the permanent magnetic field in this case leads to a 3.5-fold increase in the intensity of the main relaxation maximum and to its slight shift towards higher frequencies. Most likely, this can be due to the peculiarities of the electron spectrum during photoelectretation. This is confirmed by the illumination of this clathrate, which leads to an increase in $-\mathrm{Im}(Z\omega)$ with increasing frequency, and the relaxation maximum shifts beyond the high-frequency range of measurements.

The confirmation of the above statements is obtained by displaying the Nyquist diagrams for the initial 4-fold expanded GaSe matrix and the $\langle CS(NH_2)_2\langle C_{14}H_{10}\rangle\rangle$ clathrate formed on its basis presented in Fig. 7. While analyzing the measurement results for the initial 4-fold expanded GaSe matrix, we observe a typical view (Fig. 7a, curve 1). The Nyquist diagram is a semicircle, which, when modeled, is a parallel connection of resistance R and capacitance C, characterizing the resistance of the stage of transfer of electric charge and its accumulation. A similar behavior of the impedance hodograph is obtained by applying a permanent magnetic field, which leads to more than 2-fold reduction of both the real and imaginary part of the complex total impedance. The same can be seen for Nyquist diagrams measured under light illumination, which leads to more than a 5-fold reduction in both the real and imaginary part of complex impedance.

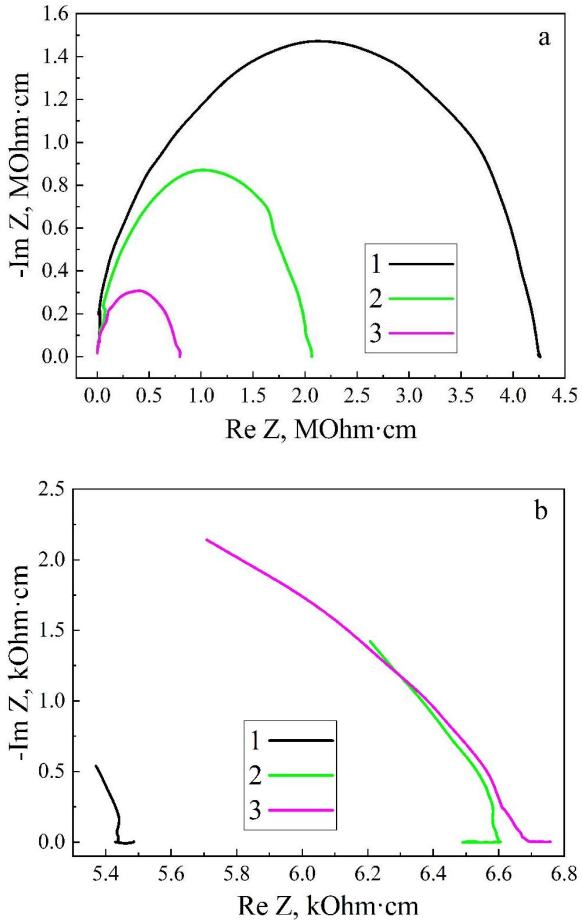

Fig. 7. Nyquist diagrams of 4-fold expanded GaSe matrix (a) and $\langle CS(NH_2)_2\langle C_{14}H_{10}\rangle\rangle$ (b). The measurements were made under normal conditions (1), in permanent magnetic field (2), and under light illumination (3)

Another view is obtained by Nyquist diagrams measured for the GaSe$\langle CS(NH_2)_2\langle C_{14}H_{10}\rangle\rangle$ clathrate (Fig. 7b), representing the form of an incomplete semicircle, which is caused by limitation of the frequency range of the measuring complex. The Nyquist diagrams measured under normal conditions visualize a low-frequency section parallel to the axis of the real part of complex resistance, directed in the direction of its growth. This behavior of the impedance hodograph in the simulation is a finite element of the constant phase (BCPE), which reflects the current in a spatially limited region with complex electrical conductivity. The application of permanent magnetic field leads to significant changes in the behavior of the complex resistance only in the low-frequency range, in which the area with the

opposite frequency genesis is visualized for the corresponding area for measurements under normal conditions. This behavior of the impedance hodograph in the simulation is represented by quantum capacitance C_q, which is connected in parallel to the series-connected resistors R and capacitance C. Illumination eliminates the manifestation of quantum capacitance and restores the low-frequency behavior of the impedance hodograph characteristic of measurements under normal conditions.

The current-voltage (CV) characteristic was also measured for the $\langle CS(NH_2)_2\langle C_{14}H_{10}\rangle\rangle$ clathrate (Fig. 8b) and acquired an extraordinary form, which is a hysteresis, in contrast to the linear behavior inherent in the initial 4-fold expanded GaSe matrix (Fig. 8a). This behavior of the CV characteristic curve may be the result of the formation of internal electret polarization. As a result, the current carriers are redistributed and the system can be charged. The corresponding hysteresis behavior remains unchanged with the application of the permanent magnetic field as well as with light illumination. This effect can be important in practice for the implementation of a new type of memory element – memristors [36]. In the literature, this phenomenon is known as the memristive effect.

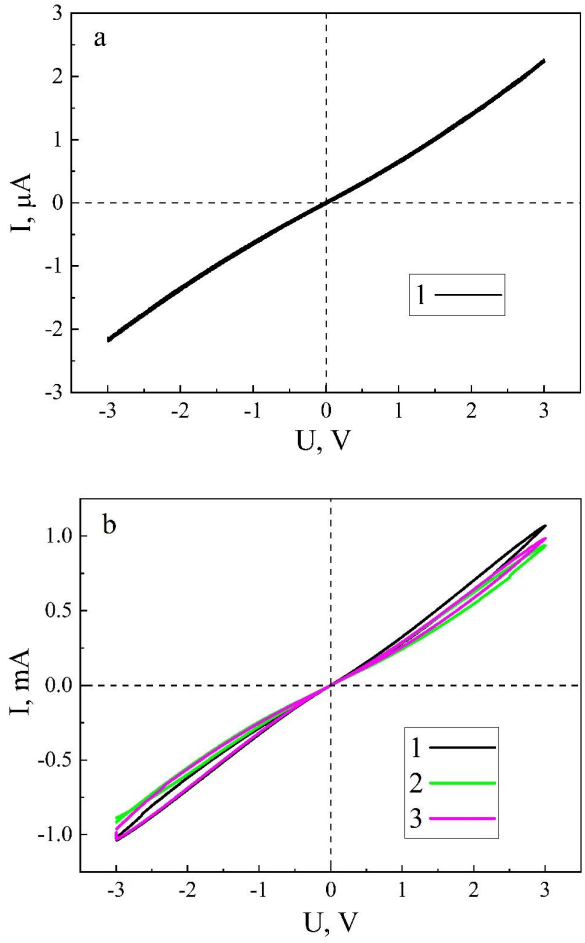

Fig. 8. The current-voltage characteristic was measured for the 4-fold expanded GaSe matrix (a) and GaSe$\langle CS(NH_2)_2\langle C_{14}H_{10}\rangle\rangle$ clathrate (b) under normal conditions (1), in the permanent magnetic field (2), and under light illumination (3). Current-voltage characteristics at the scan rate of 0.050 V s^{-1}

4. CONCLUSIONS

The synthesis of clathrate $\langle CS(NH_2)_2\langle C_{14}H_{10}\rangle\rangle$ with the imposition of illumination generates photoelectret states, which are appropriately placed in the band gap and cause the Fermi level to rise, thereby increasing conductivity.

The $\langle CS(NH_2)_2\langle C_{14}H_{10}\rangle\rangle$ clathrate formed is characterized by homo-charge relaxation and a quasi-continuous spectrum of impurity levels at the Fermi level.

Anomalous photoresistive behavior, namely, an increase in ReZ by 24% upon illumination, is observed for the synthesized clathrate GaSe$\langle CS(NH_2)_2\langle C_{14}H_{10}\rangle\rangle$. Leveling of photosensitivity of the GaSe crystal matrix can also be observed, most likely due to the specific energy structure of the clathrate, whose illumination leads to photoactivation of the acceptor centers on the inorganic/organic hetero-boundaries.

The imposition of a permanent magnetic field when measuring Re$Z(\omega)$ of $\langle CS(NH_2)_2\langle C_{14}H_{10}\rangle\rangle$ clathrate leads to the appearance of quantum capacitance (C_q). The occurrence of the latter is caused by discretization of the energy spectrum of the clathrate and finiteness of the tunneling times. This result has an important practical aspect: the generation of C_q by a permanent magnetic field.

The voltage-current characteristic measured for the GaSe $\langle CS(NH_2)_2\langle C_{14}H_{10}\rangle\rangle$ clathrate is of the hysteresis type, which results from the formation of internal electret polarization. This effect is important for the application of a new type of memory elements – memristors.

REFERENCES

[1] V. Ramamurthy and B. Mondal, "Supramolecular photochemistry concepts highlighted with select examples," *J. Photochem. Photobiol. C: Photochem Rev.*, vol. 23, pp. 68–102, 2015, doi: 10.1016/j.jphotochemrev.2015.04.002.

[2] D.B. Amabilino, D.K. Smith, and J.W. Steed, "Supramolecular materials," *Chem. Soc. Rev.*, vol. 46, pp. 2404–2420, 2017, doi: 10.1039/C7CS00163K.

[3] P. Hashim, J. Bergueiro, E. Meijer, and T. Aida, "Supramolecular Polymerization: A Conceptual Expansion for Innovative Materials," *Prog. Polym. Sci.*, vol. 105, p. 101250, 2020, doi: 10.1016/j.progpolymsci.2020.101250.

[4] T. Yu, Z.X. Shen, W.S. Toh, J.M. Xue, and J. Wang, "Size effect on the ferroelectric phase transition in $SrBi_2Ta_2O_9$ nanoparticles," *J. Appl. Phys.*, vol. 94, no. 1, pp. 618–620, 2003, doi: 10.1063/1.1583146.

[5] M.B. Smith *et al.*, "Crystal Structure and the Paraelectric-to-Ferroelectric Phase Transition of Nanoscale $BaTiO_3$", *J. Am. Chem. Soc.*, vol. 130, no. 22, pp. 6955–6963, 2008, doi: 10.1021/ja0758436.

[6] M.B. Dung and N.H. Thuong, "Phase transition and dielectric relaxation of a mixed ferroelectric composite from cellulose nanoparticles and triglycine sulfate," *Ferroelectrics*, vol. 550, no 1, pp. 141–150, 2019, doi: 10.1080/00150193.2019.1652504.

[7] M. Urdampilleta *et al.*, "Supramolecular spin valves," *Nat. Mater.*, vol. 10, pp. 502–506, 2011, doi: 10.1038/nmat3050.

[8] T. Nasobe *et al.*, "Organization of supramolecular assemblies of fullerene, porphyrin and fluorescein dye derivation on TiO_2 nanoparticles for light energy conversion," *Chem. Phys.*, vol. 319, pp. 243-252, 2005, doi: 10.1016/j.chemphys.2005.06.035.

[9] J. Roncali *et al*., "Molecular and supramolecular engineering of π-conjugated systems for photovoltaic conversion," *Thin Solid Films,* vol. 511–512, pp. 567–575, 2006, doi: 10.1016/j.tsf.2005.12.014.

[10] V. Maksymych, D. Całus, F. Ivashchyshyn, A. Pidluzhna, P. Chabecki, and R. Shvets, "Quantum energy accumulation in semiconductor⟨ionic liquid⟩ layered clathrates," *Appl. Nanosci.*, vol. 12, pp. 1147–1153, 2022, doi: 10.1007/s13204-021-01763-1.

[11] I.I. Grygorchak, F.O. Ivashchyshyn, A.K. Borysiuk, R.Ya. Shvets, and Yu.O. Kulyk, "Clathrate semiconductor multiferroics, synthesized in system GaSe–$NaNO_2$–$FÍSO_4$ and influence of cointercalation," *Radio Electron. Comput. Sci. Control*., vol. 3, pp. 7–19, 2017, doi: 10.15588/1607-3274-2017-3-1.

[12] J.-H. Choy, "Intercalative route to heterostructured nanohybrid," *J. Phys. Chem. Solids,* vol. 65, no. 2–3, pp. 373–383, 2004, doi: 10.1016/j.jpcs.2003.10.047.

[13] G. Choi, S. Eom, A. Vinu, and J.-H. Choy, "2D Nanostructured Metal Hydroxides with Gene Delivery and Theranostic Functions," *Compr. Rev, Chem. Rec.*, vol. 18, no. 7–8, pp. 1033–1053, 2018, doi: 10.1002/tcr.201700091.

[14] F.O. Ivashchyshyn, O.V. Balaban, and I.I. Grygorchak, "Peculiarities of properties of the GaSe(InSe)<$CS(NH_2)_2$> nanohybrids, synthesized under lighting," *J. Nano- Electron. Phys.*, vol. 8, no. 4, p. 04015(1–6), 2016, doi: 10.21272/jnep.8(4(1)).04015.

[15] J. Jasiński, M. Kozakiewicz, and M. Sołtysik, "The Effectiveness of Energy Cooperatives Operating on the Capacity Market," *Energies*, vol. 14, p. 3226, 2021, doi: 10.3390/en14113226.

[16] Y. Mysak, O. Pona, S. Shapoval, M. Kuznetsova, and T. Kovalenko, "Evaluation of energy efficiency of solar roofing using mathematical and experimental research," *East.-Eur. J. Enterpr. Technol.*, vol. 3, pp. 26–32, 2017, doi: 10.15587/1729-4061.2017.103853.

[17] J. Inarrea, "Microscopic theory for radiation induced zero-resistance states in 2D electron systems: Frank-Condon blockads," *Appl. Phys. Lett*., vol. 110, p. 143105, 2017, doi: 10.1063/1.4979830.

[18] D.A. Bandurin *et. Al.*, "High electron mobility, quantum Hall effect and anomalous optical response in atomically thin InSe," *Nat. Nanotechnol. Lett.*, vol. 12, no. 3, pp. 223–227, 2016, doi: 10.1038/NNANO.2016.242.

[19] I. Mora-Sero and J. Bisquert, "Implications of the Negative Capacitance Observed at Forwars Bias in Nanocomposite and Polycrystalline Solar Cells," *Nano Lett.*, vol. 6, no. 4, pp. 640 – 650, 2006, doi: 10.1021/nl052295q.

[20] N.T. Hung, A.R.T. Nugraha, and R. Saito, "Two-dimensional InSe as a potential thermoelectric materials," *Appl. Phys. Letters*, vol. 111, no. 9, p. 092107, 2017, doi: 10.1063/1.5001184.

[21] A. K. Geim and I.V. Grigorieva, "Van der Waals Heterostructures," *Nature*, vol. 499, p. 419, 2013, doi: 10.1038/nature12385.

[22] F. Huang, Z. Li, and H. Jiang, "Analysis and control of thiourea content in ammonium containing zinc plating bath," *Cailiao Baohu* vol. 30, pp. 23–25, 1997.

[23] D. Mullen and E. Hellner, "A Simple Refinement of Density Distributions of Bonding Electrons. IX. Bond Electron Density Distribution in Thiourea, $CS(NH_2)_2$, at 123K," *Acta Crystallogr*, vol. 9, pp. 2789–2794, 1978, doi: 10.1107/S0567740878009243.

[24] K. Takemoto, N. Sonoda, *Inclusion Compounds of Urea, Thiourea and Seleneurea, Inclusion Compounds*, IJ.L. Atwood, J.E.D. Davies, and D.D. MacNicol (Eds.), vol. 2, pp. 47–67, 1984.

[25] T. Pluta and A.J. Sadlej, "Electric properties of urea and thiourea," *J. Chem. Phys.*, vol. 114, no. 1, pp. 136–146, 2001, doi: 10.1063/1.1328398.

[26] C. Puzzarini, "Molecular Structure of Thiourea," *J. Phys. Chem. A*, vol. 116, pp. 4381–4387, 2012, doi: 10.1021/jp301493b.

[27] S. Kausar, A.A. Altaf, M. Hamayun, A. Badshah, and A. Razzaq, "Supramolecular Chemistry and DNA Interaction Studies of Ferrocenyl Ureas and Thioureas," in *Photophysics, Photochemical and Substitution Reactions – Recent Advances*. London, United Kingdom: IntechOpen, 2020, doi: 10.5772/intechopen.84412.

[28] X. Shang, Z. Yang, J. Fu, P. Zhao, and X. Xu, "The Synthesis and Anion Recognition Property of Symmetrical Chemosensors Involving Thiourea Groups: Theory and Experiments," *Sensors*, vol. 15, no, 11, pp. 28166–28176, 2015, doi: 10.3390/s151128166.

[29] A.J. Goshe, I.M. Steele, C. Ceccarelli, A.L. Rheingold, and B. Bosnich, "Supramolecular recognition: On the kinetic lability of thermodynamically stable host–guest association complexes," *Proceedings of the National Academy of Sciences*, 2022, vol. 99, no. 8, pp. 4823–4829, doi: 10.1073/pnas.052587499.

[30] I. Grygorchak, F. Ivashchyshyn, P. Stakhira, R.R. Reghu, V. Cherpak, and J.V. Grazulevicius, "Intercalated Nanostructure Consisting of Inorganic Receptor and Organic Ambipolar Semiconductor," *J. Nanoelectron. Optoelectron.*, vol. 8, pp. 292–296, 2013, doi: 10.1166/jno.2013.1464.

[31] R. Andreichin, "High-field polarization, photopolarization and photoelectret properties of high-resistance amorphous semiconductors," *J.Electrostat.*, vol. 1, pp. 217–230, 1975, doi: 10.1016/0304-3886(75)90018-2.

[32] J.F. Fowler, "X-Ray induced conductivity in insulating materials," *Proc. R. Soc. Lond. A.*, vol. 236, pp. 464–480, 1956, doi: 10.1098/ rspa.1956.0149.

[33] B. Lukiyanets and D. Matulka, "Quantum Capacitance of Nanoplates in Magnetic Field," *Int. J. Nanosci.*, vol. 15, p. 1650009, 2016, doi: 10.1142/s0219581x16500095.

[34] V. Parkash and A.K. Goel, "Quantum Capacitance Extraction for Carbon Nanotube Interconnects," *Nanoscale Res. Lett.*, vol. 5, no. 9, pp. 1424–1430, 2010, doi: 10.1007/s11671-010-9656-4.

[35] M. Pollak and T.H. Geballe, "Low-Frequency Conductivity Due to Hopping Processes in Silicon," *Phys. Rev.*, vol. 6, p. 1743, 1961, doi: org/10.1103/physrev.122.1742.

[36] G.U. Kamble *et al.*, "Coexistence of filamentary and homogeneous resistive switching with memristive and meminductive memory effects in Al/MnO_2/SS thin film metal–insulator–metal device," *Int. Nano Lett.*, 2018, doi: 10.1007/s40089-018-0249-z.